Fig. 3 shows the DC drain I/V characteristics for both DG and SG $0{\cdot}7 \times 200\,\mu m^2$ TEGFETs. The relatively weak kink effect observed on the SG devices almost disappears for the

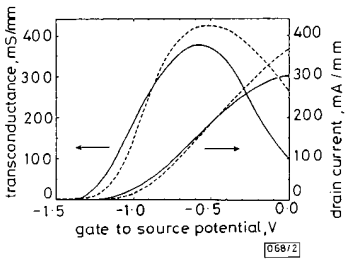

Fig. 2 *Transfer characteristics of dual-gate and single-gate $0{\cdot}7 \times 200\,\mu m^2$ TEGFETs*
——— dual-gate: $V_{DS} = 2$ V
– – – – single-gate: $V_{DS} = 1$ V

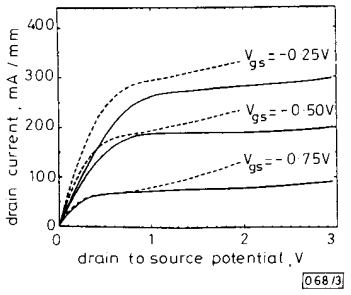

Fig. 3 *Output characteristics of dual-gate and single-gate $0{\cdot}7 \times 200\,\mu m^2$ TEGFETs*
——— dual-gate
– – – – single-gate

DG structure and the transconductance to output conductance ratio (g_m/g_D) increases from approximately 12 to values as high as 100. The DG TEGFETs characteristics at low frequencies are well described by a simple four-element small signal model, consisting of two separate voltage controlled current sources in series, each having its own parallel conductance. The measured g_D at microwave frequencies, defined by the real part of y_{22} in the admittance matrix, is less than half that at DC and remains constant from 18 GHz down to less than 0·5 GHz. The output conductance is partly caused by the real space transfer of carriers from the channel into the high-bandgap material. The observed frequency dependence of g_D is attributed to slow capture and emission processes by trap centres in the InAlAs layer.[8]

Fig. 4 shows the RF current gain, defined by $|h_{21}|$ in the hybrid matrix, and maximum stable or available power gain (MSG/MAG) from 1 to 18 GHz for the $0{\cdot}7 \times 200\,\mu m^2$ DG TEGFET at 110 mA/mm drain current. The peak f_T lies at 33 GHz and is attained at a lower drain current than that for the peak g_m. Compared with SG TEGFETs at 220 mA/mm

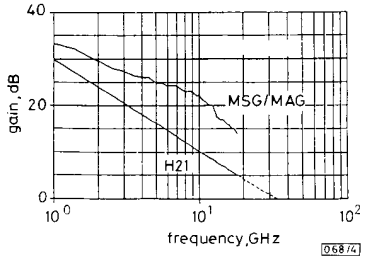

Fig. 4 *Current and maximum stable or available gain against frequency*
$0{\cdot}7 \times 200\,\mu m^2$ dual-gate TEGFET $I_D = 110$ mA/mm; $V_{DS} = 2$ V

drain current, typically 2 dB are lost on $|h_{21}|$ and 6 dB gained on MSG/MAG.

By moving the threshold voltage down to $-1{\cdot}6$ V instead of $-1{\cdot}3$ V on the same epilayer, adequate bias conditions for the channel under the first gate of the DG TEGFET and gain more than 10 dB on the MSG/MAG compared with the SG device under the same bias conditions, i.e. 220 mA/mm drain current, are expected.

Conclusions: The three-terminal dual-gate InAlAs/InGaAs TEGFET has been shown to exhibit superior performance characteristics in terms of g_m/g_D ratio and RF power gain compared with its single gate counterpart fabricated on the same wafer. A further optimisation of the threshold voltage should allow higher RF power gain, maintaining the convenient three-terminal configuration.

Acknowledgment: This work was supported by Thomson-CSF (France).

F. GUEISSAZ
R. HOUDRÉ
M. ILEGEMS

Institut de Micro- et Optoèlectronique
Ecole Polytechnique Fédérale
CH 1015 Lausanne, Switzerland

29th January 1991

References

1 BROWN, A. S., MISHRA, U. K., HENIGE, J. A., and DELANEY, M. J.: 'The impact of epitaxial layer design and quality on GaInAs/AlInAs high-electron-mobility transistor performance', *J. Vac. Sci. Technol.*, 1988, **B6**, (2), pp. 678–681
2 BANDY, S., NISHIMOTO, C., HYDER, S., and HOOPER, C.: 'Saturation velocity determination for $Ga_{0.47}In_{0.53}As$ field-effect transistors', *Appl. Phys. Lett.*, 1981, **38**, (10), pp. 817–819
3 GHOSAL, A., CHATTOPADHYAY, D., and PURKAIT, N. N.: 'Hot-electron velocity overshoot in $Ga_{0.47}In_{0.53}As$', *Appl. Phys. Lett.*, 1984, **44**, (8), pp. 773–774
4 ITOH, T., GRIEM, T., WICKS, G. W., and EASTMAN, L. F.: 'Sheet electron concentration at the heterointerface in $Ga_{0.47}In_{0.53}As/Al_{0.48}In_{0.52}As$ modulation-doped structures', *Electron. Lett.*, 1985, **21**, (9), pp. 373–374
5 PEOPLE, R., WECHT, K. W., ALAVI, K., and CHO, A. Y.: 'Measurements of the conduction-band discontinuity of molecular beam epitaxial grown $Ga_{0.47}In_{0.53}As/Al_{0.48}In_{0.52}As$, N-$n$ heterojunction by C-V profiling', *Appl. Phys. Lett.*, 1983, **43**, (1), pp. 118–120
6 LIECHTI, C. A.: 'Performance of dual-gate GaAs MESFET's as gain controlled low noise amplifiers and high speed modulators', *IEEE Trans.*, 1975, **MTT-23**, (6), pp. 461–469
7 TURNER, J. A., WALLER, A. J., KELLY, E., and PARKER, D.: 'Dual-gate GaAs microwave field-effect transistor', *Electron. Lett.*, 1971, **7**, (22), pp. 661–662
8 PALMATEER, L. F.: PhD Dissertation, Cornell University, 1989

ANALYSIS OF SIMULTANEOUS DIGITAL AND ANALOGUE SIGNAL TRANSMISSIONS IN A COHERENT OPTICAL SUBCARRIER MULTIPLEXED SYSTEM

Indexing terms: Optical communications, Multiplexers and multiplexing

The performance of the coherent subcarrier multiplexed system with mixed digital and analogue signals is analysed. The result shows that the performance of the digital channels in this system may be better than the pure digital system if the modulation index of the analogue channel is less than half of the modulation index of the digital channel. It is predicted that the system will have a 14 dB improvement over the corresponding intensity modulation/direct detection system.

Introduction: The use of microwave subcarriers in optical communication systems makes simultaneous transmissions of digital and analogue signals possible. Use of a coherent sub-

carrier multiplexed (CSCM) system to distribute either multichannel digital signals with continuous phase FSK (CPFSK) modulation or FM video channels with phase noise cancellation was reported in References 1 and 2. It is advantageous to use the CSCM system to simultaneously transmit both multichannel analogue and digital signals. The CSCM system is shown in Fig. 1. At the receiver, digital and analogue signals

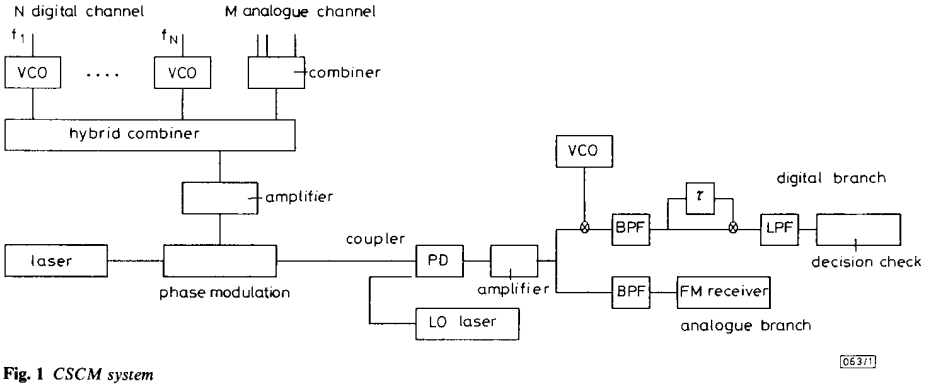

Fig. 1 *CSCM system*

are separated by the filters. The filter used in the analogue branch must have enough bandwidth to accommodate all video signals. The digital channel is selected by tuning a voltage controlled oscillator (VCO).

Analysis: At the receiver, the detected photocurrent can be written as[1]

$$i(t) = R\{P_{LO} + P_S + 2\sqrt{(P_{LO}P_S)} \times \cos[2\pi f_{IF}t + \phi_m(t)]\} + n(t) \quad (1)$$

where R is the responsivity, P_{LO} is the local oscillator (LO) power, P_S is the received signal power, f_{IF} is the intermediate frequency, $\phi_m(t)$ is phase modulation owing to the combined microwave FSK signal and FM video signal, and $n(t)$ is the shot and thermal noise. The DC terms in eqn. 1 contains no information and can be ignored. By taking the Bessel function expansion the signal of the kth channel[1] can be obtained

$$i_k(t) = AJ_1(\beta_k)\prod_{i\neq k} J_0(\beta_i) \times \cos\{2\pi[f_{IF} - f_k]t - \alpha_k(t)\} \quad (2)$$

where $A = 2R\sqrt{(P_{LO}P_S)}$, f_k is the microwave subcarrier frequency of the kth channel, $\alpha_k = 2\pi f_d \int_{-\infty}^{t} m_k(t)\,dt$, f_d is the peak frequency deviation and $m_k(t)$ is either a base-band video signal or a digital data stream. The spectrum of this photocurrent is centred at $f_{IF} - f_k$ and its amplitude is weighted by the first-order Bessel function $J_1(\beta_k)$ (for small β, $J_0(\beta) \approx 1$). Intersymbol interference and crosstalk can be ignored.[1] The availability of high quality Nd : YAG lasers,[5] and/or phase noise cancellation schemes,[2] means that the influence of phase noise can also be ignored. The CNR of the kth channel is then given by

$$\text{CNR} = \frac{\frac{A^2}{2}J_1^2(\beta_k)\prod_{i\neq k}J_0^2(\beta_i)}{\sigma_{th}^2 + \sigma_{sh}^2 + \sigma_{imd}^2} \quad (3)$$

where σ_{th}, σ_{sh} and σ_{imd} are the variances of the thermal noise, shot noise, and intermodulation distortion (IMD), respectively.

The third IMDs that fall directly in the kth channel satisfy the following condition:[1]

$$|f_{IF} - (f_h \pm f_i - f_j)| = |f_{IF} - f_k| \qquad h \neq i \neq j \quad (4)$$

The amplitudes of the third-order IMDs are weighted by $J_1(\beta_h)J_1(\beta_i)J_1(\beta_j)$. The second-order IMDs are of the form $f_i \pm f_j$ and fall directly in the desired signal band when

$$|f_{IF} - (f_i \pm f_j)| = |f_{IF} - f_k| \qquad i \neq j \quad (5)$$

The amplitude of the second-order IMDs are weighted by $J_1(\beta_i)J_1(\beta_j)$. The second-order IMDs affect the system much more than the third-order IMDs because of their larger amplitude.

Example: Consider a system containing 17 digital channels and 12 analogue video channels with the frequency allocation shown in Fig. 2. The digital channels are allocated from 2·1 GHz to 3·7 GHz and from 4·5 GHz to 5·9 GHz with 120 MHz bandwidth and 80 MHz guardband. The 12 FM video channels are allocated from 3·88 GHz to 4·32 GHz. Each digital channel has a 100 Mbit/s baseband data rate. Each analogue channel carries 30 MHz FM TV signal and has a 10 MHz guardband. This frequency allocation is similar to that in References 1–3 but replaces the middle three channels with analogue channels. In this frequency allocation, analogue channels are least affected by the second-order IMD and produce the least second-order IMD.

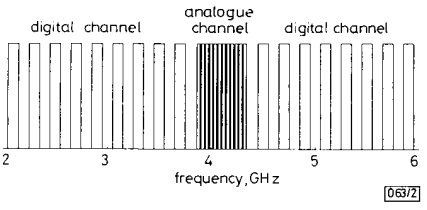

Fig. 2 *Frequency allocation of CSCM system*

The worst channels will be the first digital channel and the first analogue channel because of the second-order IMDs. Compare the σ_{imd} of the system with that in Reference 1: the performance of the digital channel in the system will be better than that in Reference 1 if $\beta_a/\beta_d < 0{\cdot}43$. When the intersymbol interference and phase noise are ignored, the CNR must be greater than 16·3 dB for a CPFSK system to achieve the bit error rate (BER) $< 10^{-9}$.[6] For the FM-TV signal, $CNR \geq 17$ dB is required to achieve a SNR ≥ 56 dB.[2,4] The BER of the first digital channel and CNR of the first analogue channel are shown in Fig. 3. Several values of β_a are chosen to show the effect of the analogue channels on the digital channel. It is seen that with $\beta_a = 0{\cdot}1$, the system is overmodulated and a BER floor appears. When $P_s = -30$ dBm and $P_{LO} = 1$ mW, $\beta_d = 0{\cdot}1$, $\beta_a = 0{\cdot}05$ may be chosen to achieve a BER $< 10^{-9}$ and SNR > 56 dB.

Fig. 4 shows the range of β in which the system can simultaneously achieve BER $< 10^{-9}$ for the digital channel and SNR > 56 dB for the analogue channel. The minimum received optical signal power is $P_{S_{min}} = -30{\cdot}4$ dBm with $\beta_d = 0{\cdot}115$, $\beta_a = 0{\cdot}05$, which is comparable with the optimal transmission condition in Reference 1.

Conclusion: The performance of a CSCM system when multichannel digital and analogue signals are simultaneously trans-

mitted has been analysed. The system can work well with appropriate β_a and β_d as shown in Fig. 4. If the system is designed according to the rule presented ($\beta_a < 0{\cdot}43\beta_d$), it will

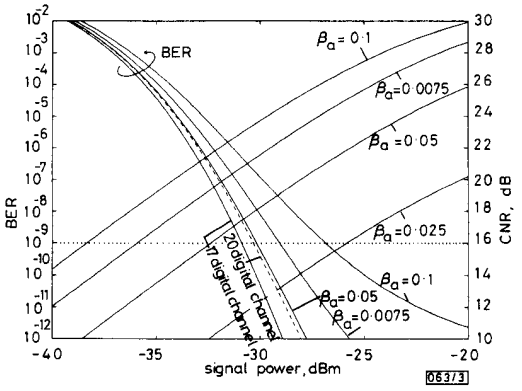

Fig. 3 *BER and CNR of first digital channel and first video channel*
$P_{LO} = 1\,\text{mW}; \beta_d = 0{\cdot}1$
Also shown is BER of first channel of 20 digital-channel system

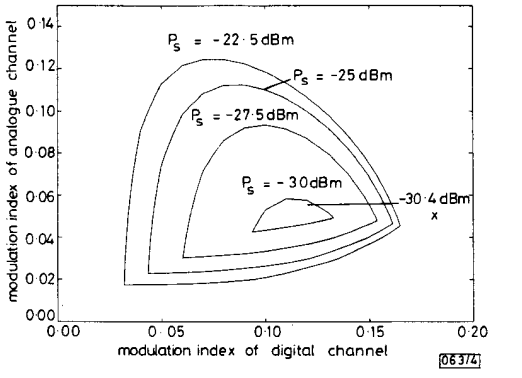

Fig. 4 *Range in which BER $< 10^{-9}$ for digital channels and SNR > 56 dB for analogue channels*

have a 14 dB (or a little more) improvement over the corresponding intensity modulation/direct detection (IM/DD) system. The example shows that for a system with 17 digital channels and 12 analogue channels, the receiver sensitivity can reach −30 dBm.

J. WU
H.-W. TSAO
K.-P. HO
Y.-H. LEE

Department of Electrical Engineering
National Taiwan University
Taipei, Taiwan 10764, Republic of China

28th January 1991

References

1 GROSS, R., and OLSHANSKY, R.: 'Multichannel coherent FSK experiment using subcarrier multiplexing techniques', *J. Lightwave Technol.*, 1990, **LT-8**, pp. 406–415
2 OLSHANSKY, R., GROSS, R., and SCHMIDT, M.: 'Subcarrier multiplexed coherent lightwave systems for video distribution', *IEEE J. Sel. Areas Commun.*, 1990, **SAC-8**, pp. 1268–1275
3 HILL, P. M., and OLSHANSKY, R.: 'A 20-channel optical communication system using sub-carrier multiplexing for the transmission of digital video signals', *J. Lightwave Technol.*, 1990, **LT-8**, pp. 554–560
4 WAY, W. I.: 'Subcarrier multiplexed lightwave system design considerations for subscriber loop applications', *J. Lightwave Technol.*, 1989, **LT-7**, pp. 1806–1818
5 KAZOVSKY, L. G., and ATLAS, D. A.: 'Miniature Nd : YAG lasers: noise and modulation characteristics', *J. Lightwave Technol.*, 1990, **LT-8**, pp. 294–301
6 KAZOVSKY, L. G., and JACOBSEN, G.: 'Multichannel CPFSK coherent optical communication systems', *J. Lightwave Technol.*, 1989, **LT-7**, pp. 972–982

PRODUCT AND INTERLEAVING OF ANTICODES

Indexing terms: Code convertors, Codes and coding

Two techniques are presented for constructing new anticodes from known anticodes, namely the product and interleaving of anticodes. The product of anticodes (m_1, k_1, δ_1) and (m_2, k_2, δ_2) produces an (m_1m_2, k_1k_2, δ) anticode, where $\delta_1\delta_2 \leq \delta \leq \min[m_1\delta_2, m_2\delta_1]$. Interleaving of degree λ of an (m, k, δ) anticode produces an $(m\lambda, k\lambda, \delta\lambda)$ anticode. The efficiency of these constructions is examined in terms of the Griesmer bound for the binary case. As a result a rule is derived for selecting anticodes which can be efficiently combined either by product or interleaving.

Introduction: The anticode concept[1] has been successfully employed to find optimum error-correcting codes by deletion of columns from an m-sequence codebook.[2] A q-ary anticode AC (m, k, δ) is defined as a rectangular array of GF(q) symbols, with N rows and m columns, having a maximum Hamming distance δ between any pair of rows. Each row in the array represents an anticodeword of length m. The linear anticodes, considered in the sequel, are obtained when the array forms a group[2] and in this case $N = q^k$. The properties of an anticode are complementary to those of a code.

Two techniques are presented for constructing new anticodes from known anticodes, namely the product and interleaving of anticodes. Both techniques have long been used in the context of error-correcting codes.[2] Their use for constructing anticodes is new. The efficiency of these constructions is examined in terms of the Griesmer bound in the binary case. A rule is derived for selecting anticodes which can be efficiently combined either by product or interleaving. Optimal or near optimal anticodes, in the sense of having the lowest maximum distance δ for given values of m and k,[1] can thus be obtained.

Product anticodes: Given two anticodes AC_1 and AC_2 with parameters (m_1, k_1, δ_1) and (m_2, k_2, δ_2), respectively, a product anticode is defined by its anticodewords as follows: The product anticodewords are represented by a two-dimensional array containing m_2 rows and m_1 columns, where the rows are anticodewords of AC_1 and the columns are anticodewords of AC_2. The maximum distance of a product anticode can be upperbounded and lowerbounded as shown in theorem 1.

Theorem 1: The maximum distance δ of a product anticode derived from anticodes AC_1 and AC_2 with parameters (m_1, k_1, δ_1) and (m_2, k_2, δ_2), respectively, is bounded by

$$\delta_1\delta_2 \leq \delta \leq \min[m_1\delta_2, m_2\delta_1] \quad (1)$$

Proof: The upperbound on δ is proved as follows: The total weight W of the rectangular array formed with AC_1 and AC_2 will be calculated in two different ways. First, by adding the m_1 array columns, which are anticodewords from AC_2, the result is

$$W \leq m_1\delta_2 \quad (2)$$

The reason for the inequality sign in eqn. 2 is because not all the anticodewords of AC_2 necessarily have weight δ_2. Second, in a similar manner, by adding the m_2 array rows, which are anticodewords from AC_1, the result is

$$W \leq m_2\delta_1 \quad (3)$$